Polyhedron 52 (2013) 62–71

Contents lists available at SciVerse ScienceDirect

Polyhedron

journal homepage: www.elsevier.com/locate/poly

Evaluation of the potential effectiveness of ruthenium(II) complexes with 2,3-disubtituted pyrazino[2,3-f][1,10]phenanthroline anchors, R_2ppl (R = CN, COOH, COOEt, OH) as sensitizers for solar cells

Angélica Francois [a,*], Ramiro Díaz [a], Angélica Ramírez [a], Bárbara Loeb [b], Mauricio Barrera [b], Irma Crivelli [c]

[a] Facultad de Ciencias, Universidad Católica de Temuco, Rudecindo Ortega 02950, Temuco, Chile
[b] Facultad de Química, Pontificia Universidad Católica de Chile, Vicuña Mackenna 4860, Santiago, Chile
[c] Facultad de Ciencias, Universidad de Chile, Las Palmeras 3425, Santiago, Chile

ARTICLE INFO

Article history:
Available online 14 December 2012

Keywords:
R_2ppl ligand
Ruthenium complexes
Acceptor ligand
TDDFT calculations

ABSTRACT

The ligands of type pyrazino[2,3-f][1,10]phenanthroline, R_2ppl, with R = CN, COOH, COOEt or OH, were synthesized and used as precursors for obtaining the corresponding series of complexes of type $[Ru(dmbpy)_2R_2ppl](PF_6)_2$, where *dmbpy* is 4,4′-dimethyl-2,2′-bipyridine. The compounds were prepared, characterized, and studied by theoretical DFT calculations in order to evaluate their potentiality as dyes in photoelectrochemical cells.

The electron acceptor capacity of the R_2ppl ligands was evaluated by analyzing parameters such as electrophilicity and charge distribution on the reduced ligand. Additionally, the R substituents on R_2ppl were evaluated as anchoring groups, by variables such as highest spin occupied molecular orbital (HSOMO). Finally, the I_T parameter was defined and calculated. This is related to the amount of energy that can be delivered to TiO_2 from the acceptor anchoring ligand in the *thexi* state. According to this parameter, the $[Ru(dmbpy)_2(COOH)_2ppl](PF_6)_2$ complex is predicted to have the best response, among the compounds of the series, when used as dye in a solar cell.

1. Introduction

Intense research in the context of renewable energy has led to the development of a series of metal complexes with potential application as dyes in solar photoelectrochemical cells (DSSCs). DSSCs are based on the sensitization to visible light of mesoporous, nanocrystalline semiconductor metal oxide films achieved by means of the adsorption of molecular dyes [1–4]. Photoinduced electron injections from the sensitizer dye into the metal oxide conduction band generate charge separated states; the electrons are injected through an anchoring group into the dye [5]. In this way, the processes of electron injection into the semiconductor conduction band and of absorption of visible and near infrared light become independent [6].

One of the important variables to optimize and to control in solar photoelectrochemical cells is the anchor [7], through which the dye is fixed to the semiconductor. The electron injection to the semiconductor through the anchor is the most Commonly invoked mechanism for this process [8]. In this context, several studies have been reported, where an optimization of the anchor is sought, mostly to improve the anchor–semiconductor connection [5,7,9]. This aim implies to consider not only electronic aspects but also the efficient and stable adsorption of the dye on the semiconductor surface [10].

One of the best solar-to-electric power conversion efficiency in DSSCs has been achieved with polypyridyl complexes of ruthenium(II) [11] and osmium(II) [12] bearing carboxylated ligands as anchors, which are often employed as TiO_2 sensitizers in such cells. These species give rise to intense visible metal-to-ligand charge transfer (MLCT) bands with a favorable energetics for charge injection. 4,4′-Dicarboxylic acid-2,2′-bipyridine type ligands have been mostly used as anchors [13]. As an alternative possibility, in the present work 2,3-disubstituted pyrazino-[2,3-f][1,10]phenanthroline, R_2ppl, with R = CN, COOH, COOEt and OH were evaluated as potential anchoring groups in Ru complexes. The synthesized complexes were of $[Ru(dmbpy)_2R_2ppl](PF_6)_2$ type, Scheme 1, where *dmbpy* is 4,4′-Dimetyl-2,2′-bipyridine.

Specifically, the spectroscopic and electrochemical properties of complexes **1**–**4** were studied in order to evaluate the effects of the R substituents on the electronic properties of the complexes. The latter were characterized and studied by commonly used experimental techniques. Theoretical DFT calculations allowed an understanding of the electronic distribution in ligands and complexes. Finally, a theoretical parameter, I_T, was introduced, in order to evaluate the amount of electronic density available at the

* Corresponding author.
E-mail address: anfranci@uct.cl (A. Francois).

0277-5387/$ - see front matter © 2012 Elsevier Ltd. All rights reserved.
http://dx.doi.org/10.1016/j.poly.2012.12.003

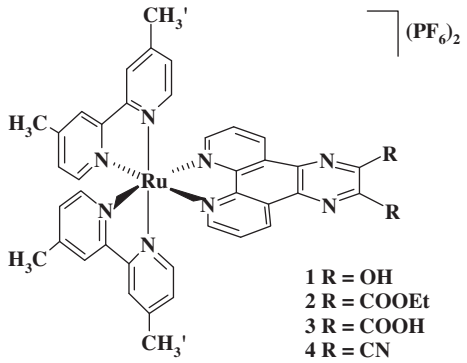

Scheme 1.

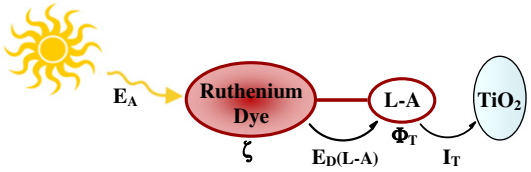

Fig. 1. Schematic representation of the energy flow in a DSSC. Parameters are defined in Section 4.

anchoring ligand, which is delivered to the TiO_2 semiconductor conduction band. This parameter should be indicative of the injection capacity of the proposed dye, as can be seen in Fig. 1, which describes the energy flow in a typical sensitized solar cell.

2. Experimental

2.1. Materials

Both reagents and solvents were pa grade, laboratories Sigma–Aldrich or Merck. All of them were used as purchased and, when needed, were purified and dried by standard methods. Diaminomaleonitrile and NH_4PF_6 were Sigma–Aldrich and the rest of the solid chemicals were Merck. The precursors 1,10-phenanthroline-5,6-dione (phendione) [14] and dichloro-*bis*-(4,4-dimethyl-2, 2′-bipyridine)ruthenium(II) (*cis*-Ru(dmbpy)$_2$Cl$_2$) [15] was synthesized following reported procedures. The corresponding elemental analysis and ^{1}H NMR spectra were in agreement with the published results.

2.2. Physical measurements and instrumentation

Elemental analyses were performed on a Fisons Instruments Analyzer, model EA 1108/CHNS–O with PC NCR system 3225. UV–Vis Spectra were recorded on a Shimadzu, UV-3101 PC Spectrophotometer. IR Spectra on Bruker Vector-22FTIR spectrometer using KBr pellets and ^{1}H NMR Spectra on a Bruker AC/200 (200 MHz) or Bruker Aspect 400 MHz spectrometer, using CD_3CN or $CDCl_3$ as solvent and TMS as reference. Cyclic voltammetry experiments were carried out using a BAS CV-50W-2,3-MF-9093 equipment; with a three-electrode arrangement with a platinum wire, a platinum coil and a Ag/AgCl electrode as working, auxiliary and reference electrode, respectively. Experiments were carried out in Argon atmosphere, with tetrabutylammoniumhexafluorophosphate (HBTA) 0.1 M (Aldrich) as supporting electrolyte and a scan speed of 200 mV s^{-1}.

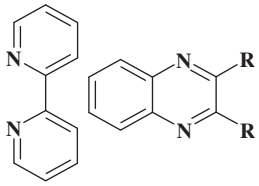

Scheme 2. Fragment decomposition of the *R$_2$ppl* ligands.

2.3. Theoretical studies

All the calculations where performed on *ADF2010* [16]. The geometrical optimization was done using DZP basis set for C, N, O, H and TZP basis set for ruthenium in combination with the PW91 exchange correlation potential [17]. One-electron properties of the ligands were determined in the gas phase using TZP basis set while charge distributions were obtained by means of the Hirshfeld method [18]. For complexes, TDDFT calculations [19] were performed using SAOP exchange correlation functional [19], SZ basis set for C, H, O, N and ZORA-TZ2P basis for ruthenium. Solvent effects were included through the COSMOS model [20] employing a Van der Waals surface and Bondi atomic radius.

Regarding the calculations involving ligands, it has been proposed that *R$_2$ppl* type ligands can be described as being formed by two fragments, either (phenanthroline(F) + pyrazine (P)) or (bypiridine (B) + quinoxaline (Q)). The latter ligand partitioning, Scheme 2, was applied in the calculations, since it permits a clear understanding of the effect of R, in particular on the electron donor/acceptor capacity of the ligand, and on the composition of the LUMO orbital for the free and complexed ligands.

In this paper a theoretical model that enables the calculation of the amount of absorbed energy effectively transmitted to the acceptor anchoring ligand is proposed. In this ligand, the R substituent plays two roles: first as an anchoring group, providing a physical linkage between the ruthenium complex and the semiconductor – usually titanium dioxide – surface. Second, it acts as a wire, conducting electronic charge from the dye to the semiconductor conduction band. The proposed model can be classified as "non-interacting" since it considers that the spectroscopic properties of the dye are not modified when it is bound to the semiconductor layer, and that the molecular orbital order and composition of the complexes will remain unaffected by the presence of the titanium dioxide orbitals.

The amount of energy (I_T) that can be delivered to TiO_2 from the acceptor anchoring ligand (LA) in the electronic thermally equilibrated, *thexi*, state *T*, is calculated in terms of absorbed energy (E_A), and, the delivered energy (E_D) to a specific fragment of the molecule, Fig. 2. ζ(LA) and Φ_T(A) are distribution functions taking into account the contribution of the LA ligand to the excited state density, and the contribution of the anchor to the T excited state [21]. The value of $E_A\zeta$(LA) is the amount of electronic density delivered to the ligand when composed by two molecular fragments L and A (in this case B and Q, Scheme 2). I_T represents the amount of absorbed energy that is channelled by the complex to the anchor group, and that can be injected into the conduction band of the semiconductor. By the MLCT absorption process, electronic density from populated d-metal orbitals is transferred to the LUMO of the acceptor anchoring ligand. The distribution of this extra charge along the different sites of the organic molecule can be studied by analysing the composition of the highest spin occupied molecular orbital (HSOMO). From this study, the role played by the different anchoring groups can be evaluated.

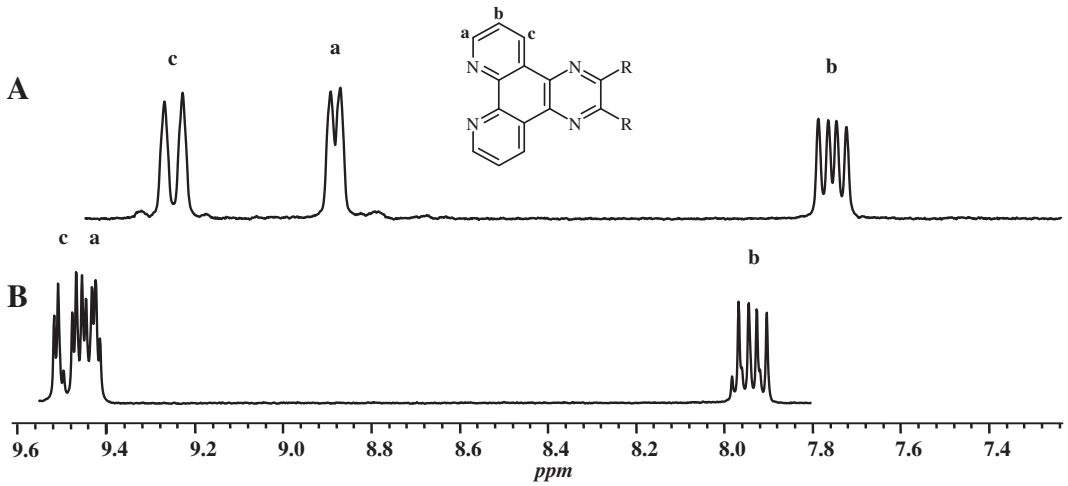

Fig. 2. ^{1}H NMR spectra of *(CN)$_2$ppl* (A) in $CDCl_3$ and *(COOH)$_2$ppl* (B) in D_2O/OD^-.

2.4. Synthesis

2.4.1. Synthesis of ligands

2,3-Dicyanopyrazino[2,3-f][1,10]phenanthroline(*(CN)$_2$ppl*): This synthesis was carried out by a reported method for unsubstituted ppl ligand [22]. The obtained results were consistent with those published [23].

Yield: 0.686 g (87%). *Anal.* Calc. for $C_{16}H_6N_6$ (M = 282.26 g/mol): C, 68.08; H, 2.14; N, 29.57. Found: C, 68.36; H, 2.07; N, 28.87%. IR (KBr pellet, cm^{-1}): 3060, 2241, 1616. ^{1}H NMR ($CDCl_3$ as solvent, δ in ppm and J in Hz): 9.50 (dd, 2H, Ha, Ha′, J_{ab} = 4.43, J_{ac} = 1.72), 7.94 (dd, 2H, Hb, Hb′, J_{ba} = 4.43, J_{bc} = 2,96), 9.60 (dd, 2H, Hc, Hc′, J_{cb} = 2.96, J_{ca} = 1.72).

2,3-Dicarboxypyrazino[2,3-f][1,10]phenanthroline(*(COOH)$_2$ppl*): 0.30 g (1.06 mmol) of *dcppl* were suspended in 30 mL of 5 M sulphuric acid and refluxed for 5 h. A white precipitate was collected by centrifugation. The solid was washed with abundant degassed water, then with ethanol and finally with ethyl ether and dried under high vacuum. Yield: 0.334 g (98%) *Anal.* Calc. for $C_{16}H_8N_4O_4$ (M = 320.26 g/mol): C, 60.00; H, 2.52; N, 17.49. Found: C, 59.88; H, 2.49; N, 17.37%. IR (KBr pellet, cm^{-1}): 3500–2600, 1741, 1619, 1415. ^{1}H NMR (D_2O (NaOD solution) as solvent, δ in ppm and J in Hz): 8.88 (d, 2H, Ha, Ha′, J_{ab} = 4.43), 7.75 (dd, 2H, Hb, Hb′, J_{ba} = 4.43, J_{bc} = 8.37), 9.50 (d, 2H, Hc, Hc′, J_{cb} = 8.37).

2,3-Diethoxycarbonylpyrazino[2,3-f][1,10]phenanthroline((COOEt)$_2$ppl): 0.23 g (0.81 mmol) of*(COOH)$_2$ppl* were dissolved in 3 mL of thionyl chloride ($SOCl_2$) under N_2 atmosphere. The solution was refluxed during 3.5 h and $SOCl_2$ in excess was eliminated under high vacuum. Then, 8.0 mL of dry ethanol was added and the mixture was refluxed overnight. A cream color precipitate of colloidal appearance was obtained and separated by centrifugation. The solid was repeatedly washed with ethyl ether and dried under high vacuum.

Yield: 0.225 g (83%), *Anal.* Calc. for $C_{20}H_{16}N_4O_4$, (M: 376.37 g/mol): C, 63.82; H, 4.28; N, 14.89. Found: C, 63.41; H, 4.1; N, 14.46%. IR (KBr pellet, cm^{-1}): 3087, 3053, 2986, 2937, 2906, 1710, 1616.

2,3-Dihydroxopyrazino[2,3-f][1,10]phenanthroline(*(HO)$_2$ppl*): 0.30 g (1.06 mmol) of *(CN)$_2$ppl* were dissolved in a hot solution of NaOH 5 M. The mixture was refluxed during 5 h. The pH was adjusted to 8–9 with 5 M H_2SO_4, a cream color precipitate of colloidal appearance being obtained. The solid was filtered off, washed with ethanol and ethyl ether and dried under high vacuum.

Yield: 0.274 g (97.7%). *Anal.* Calc. for $C_{14}H_8N_4O_2$, (M: 264.24 g/mol): C, 63.63; H, 3.05; N, 21.20. Found: C, 62.88; H, 2.97; N, 20.86%. IR (KBr pellet, cm^{-1}): 3425, 1619, 1594, 1124.

2.4.2. Synthesis of ruthenium complexes

All the complexes were synthesized using *cis*-Ru(dmbpy)$_2$Cl$_2$ as precursor. In a typical experiment, stoichiometrical quantities (~0.180 mmol) of the appropriate ligand and *cis*-Ru(dmbpy)$_2$Cl$_2$ were mixed in 1:2 ratio, in 25 mL of ethanol as solvent, and refluxed under N_2 atmosphere [22]. The solvent was reduced by rotary evaporation and 3 mL of saturated NH_4PF_6 aqueous solution were added. The red solid was isolated by filtration and purified by column chromatography (Al_2O_3; eluted with $CHCl_3$ to eliminate untreated precursor complex and then with MeOH/$CHCl_3$). Particular details for the synthesis of complexes are described below.

*[Ru(dmbpy)$_2$(OH)$_2$ppl](PF$_6$)$_2$ (**1**):* Reflux time: 8 h. *Yield*: 0.132 g (70%). Chromatographic column eluted with $CHCl_3$/MeOH 70/30. IR (KBr pellet, cm^{-1}) *ν*: 3426, 3065, 2950–2840, 1621, 1140, 844. *δ*: 1617.

*[Ru(dmbpy)$_2$(COOEt)$_2$ppl](PF$_6$)$_2$ (**2**):* Reflux time: 9 h. *Yield:* 0.140 g (66%). Chromatographic column eluted with $CHCl_3$/MeOH 60/40. IR (KBr pellet, cm^{-1}) *ν*: 3078, 2980–2900, 1720, 1612, 1240, 845.

*[Ru(dmbpy)$_2$((COOH)$_2$ppl](PF$_6$)$_2$ (**3**):* Reflux time: 8 h. *Yield:* 0.130 g (68%). Chromatographic column eluted with $CHCl_3$/MeOH 60/40. IR (KBr pellet, cm^{-1}) *ν*: 3630, 3428, 3076, 2980–2900, 1737, 1617, 845.

*[Ru(dmbpy)$_2$(CN)$_2$ppl](PF$_6$)$_2$ (**4**):* Reflux time: 6 h. *Yield:* 0.135 g (72%). Chromatographic column eluted with $CHCl_3$/MeOH 90/10. IR (KBr pellet, cm^{-1}) *ν*: 3084, 2917, 2223, 1619, 846.

3. Results and discussion

3.1. Synthesis

The synthesis of the complex *[Ru(bpy)$_2$(CN)$_2$ppl)]$^{+2}$* has been reported previously by *in situ* condensation of the [Ru(bpy)$_2$(phendione)]$^{+2}$ precursor with diaminomaleonitrile [24]. Subsequent treatment of *[Ru(bpy)$_2$(CN)$_2$ppl)]$^{+2}$* with NaOH or H_2SO_4, permits to obtain *[Ru(bpy)$_2$(OH)$_2$ppl)]$^{+2}$* and *[Ru(bpy)$_2$(COOH)$_2$ppl)]$^{+2}$*, respectively. In the present work, the *R$_2$ppl* free ligands (R = CN, OH and COOH) were synthesized prior to their coordination to Ruthenium, for their unambiguous characterization, and in order to understand the effects produced by coordination. Specifically, the synthesis of 5,6-dicianopyrazino[2,3-f][1,10]phenanthroline*(CN)$_2$ppl* was achieved following a reported procedure [22,25], but using excess phendione, thus increasing the reaction yield. The *(COOH)$_2$ppl* ligand was synthesized by hydrolysis of *(CN)$_2$ppl* in 50% sulfuric acid media [26]. The new ligand 2,3-diethoxycarbonilpyrazino[2,3-f][1,10]phenanthroline, *(COOEt)$_2$ppl*

was synthesized by esterification of *(COOH)$_2$ppl* in ethanol. Scheme 3 shows the synthesis routes for all the ligands. ^{1}H NMR, IR and Elemental Analysis results were in good agreement with the proposed formula for all the ligands.

The synthesis of the *[Ru(dmbpy)$_2$R$_2$ppl](PF$_6$)$_2$* series of complexes (R = CN, OH, COOH and COOEt) was conducted according to reported procedures for similar ruthenium polypyridine complexes [22,27], implying the substitution of chlorine in *Ru(dmbpy)$_2$Cl$_2$* by the corresponding *R$_2$-ppl* ligands. The yields for these syntheses were in the 66–72% range.

3.2. Spectroscopic properties of the free ligands

The ^{1}H NMR spectra of ligands *(CN)$_2$ppl* and *(COOH)$_2$ppl* are shown in Fig. 2. Both spectra show the same pattern with three magnetically nonequivalent protons on the bipyridine moiety, with the expected integration. The lowest field signal is assigned to protons in Hc and Hc′ positions (see Fig. 2), due to the anisotropic effect of the pyrazine N-atoms [22,28]. The Ha and Ha′ protons appear at a higher, due to the inductive effect of the phenanthroline N-atoms. The highest-field signal is assigned to protons Hb and Hb′, showing an *orto* interaction with Ha and Hc. The *(CN)$_2$ppl* ligand shows a displacement to lower field of protons Ha, Ha′; Hb, Hb′ and Hc, Hc′ when compared to the unsubstituted *ppl* ligand [28], in agreement with the electron acceptor effect of the cyano groups.

The ^{1}H NMR spectra of the *(OH)$_2$ppl* and *(COOEt)$_2$ppl* ligands was not registered because they turned out to be insoluble in all the deuterated solvents available.

The IR spectra of the free ligands show the characteristic bands of the corresponding functional groups, in addition to the ν(C–H) band *c.a.* at 3080–3000 cm^{-1}, and δ (C–H) signal *c.a.* at 1600–1620 cm^{-1}, corresponding to the aromatic hydrogen atoms of phenantroline. For the *(CN)$_2$ppl* ligand, the band at 2247 cm^{-1}, was assigned to the stretching mode of the C≡N group and shows a displacement to higher energy with regard to the diaminomaleonitrile reagent (2215 cm^{-1}). On the other hand, the ν(C=O) signal at 1685 cm^{-1}of the phendione precursor and the ν(N–H) bands at 3440 and 3300 cm^{-1} of the diaminomaleonitrile reactive were not observed. The displacement of the C≡N stretching, and the disappearance of the OH and NH bands evidence the formation of the *(CN)$_2$ppl* ligand. For the *(OH)$_2$ppl* ligand, the disappearance of the ν(C≡N) signal and the appearance of two intense signals, typical of the hydroxyl group: ν(O–H) at 3425 cm^{-1} (wide) and δ(O–H) at 1634 cm^{-1}, demonstrate that the substitution reaction was complete. In the IR spectra of the *(COOH)$_2$ppl* ligand, the carboxyl group signals highlight. The bands at 3434 and 3081 cm^{-1} are assigned to stretching modes of the free and associated O–H respectively, while the band at 1741 cm^{-1} is assigned to the stretching mode of protonated carboxyl group. The band at 1415 cm^{-1} is assigned to the stretching mode of C–O plus deformation mode of O–H. A of low intensity also appears at 1631 cm^{-1}, and is assigned to deprotonated carboxyl groups, indicating that the completely protonated ligand predominates. Besides, in the *(COOEt)$_2$ppl* ligand the aliphatic ν(C–H) *c.a.* at 2990–2850 cm^{-1} is observed, as well as a band at 1730 cm^{-1} related to the C=O stretching. The disappearance of the OH signals of the carboxyl group and the appearance of a carboxylate signal indicates the formation of the ester.

The UV–Vis spectra of the free ligands show a series bands in the UV region between 280 and 350-nm, and a strong band at 260 nm, all assigned to $\pi\rightarrow\pi^*$ transitions.

3.3. Spectroscopic properties of the complexes

It was possible to record the^{1}H NMR spectra of the four complexes synthesized, although some with low resolution due to their low solubility in the available deuterated solvents. All the spectra exhibit the signals of the *dmbpy* and *R$_2$ppl* ligands, showing good integrals correlation between the protons of the different ligands; therefore, the presence of the desired complexes can be inferred.

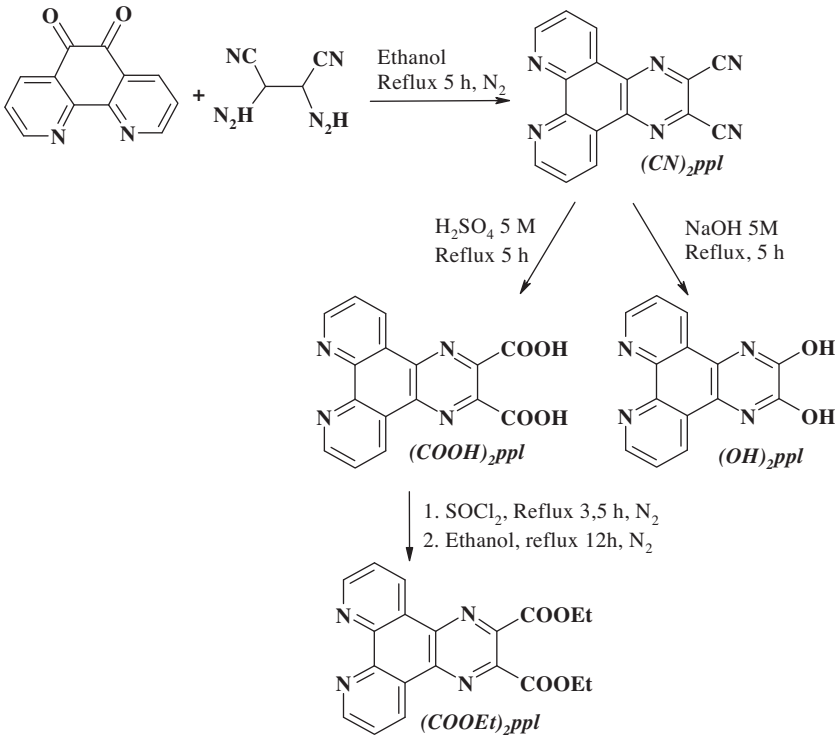

Scheme 3. Routes of synthesis of all the ligands.

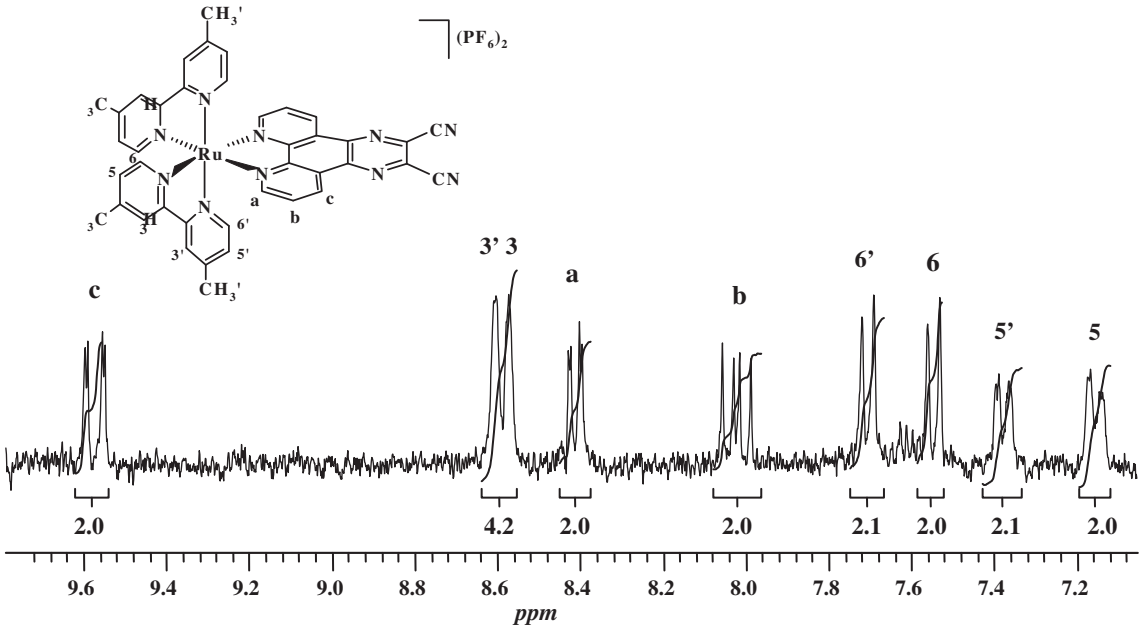

Fig. 3. Aromatic zone of ^{1}H NMR spectra of *[Ru(dmbpy)$_2$(CN)$_2$ppl](PF$_6$)$_2$*, at 400 MHz in CD_3CN.

Fig. 3 shows the spectrum of complex *[Ru(dmbpy)$_2$(CN)$_2$ppl](PF$_6$)$_2$*, **4**, while Table 1 summarizes the data obtained for all the synthesized complexes. All spectra show nine aromatic signals, corresponding to nine equivalent protons pairs. The signals were assigned by comparing them with the spectra of *(COOH)$_2$ppl* and *(CN)$_2$ppl* free ligands, and based on those coupling constants that were split Three signals are assigned to protons on the *R$_2$ppl* ligands (see Fig. 3). Since the spectra of all complexes were registered in acetonitrile-d_3 and those of the *(COOH)$_2$ppl* and *(CN)$_2$ppl* free ligands in D_2O/OD^- and chloroform-*d* respectively, it is not possible to analyze the effect of the metal on the chemical shifts of protons of these ligands in their respective complexes. Despite this, it can be observed that in complex **4** the Hb and Hc protons signals shift to lower field: 30 and 33 ppm respectively, and the Ha protons to 47 ppm, which cannot be attributed only to the solvent, but also to the deshielding effect exerted by the metal coordinated to the acceptor ligand.

The aromatic protons of the *dmbpy* ligand were assigned based on their coupling constants. In general, the H6 and H6′ protons appear as doublet signals and are not equivalent. This originates from the fact that the H6 protons are affected by the N of the *dmbpy* ligand, while the H6′ protons are affected by the N of the *R$_2$ppl* ligand. The H5′ and H5 protons are not equivalent either, for the same reason previously mentioned. These appear as doublet signals split by coupling at long distance with the H3′ and H3 protons, respectively. The H3′ and H3 protons suffer the meta effect of the N coordinated to the metal; thus they appear more deshielded and their coupling with H5′ and H5 is slightly lowered.

The IR spectra of all complexes show the C–H tension bands of the methyl groups on the *dmbpy* ligand in the 2980–2850 cm^{-1} range, and the typical signals of the PF_6^-counter ion (*c.a.* 842–848 cm^{-1}), confirming the cationic nature of the complexes. By comparison with the ring-stretching modes reported for $[Ru(bpy)_3]^{2+}$ [29] the bands at *c.a.* 1600, 1480, 1440 cm^{-1} that appear in the IR spectra of all the complexes were assigned to the ring-stretching modes of conjugated C=C bonds of the *dmbpy* ligand. Additionally, the IR spectrum of each complex shows the signals of the functional group substituted on the *ppl* ligands, with small variations with regard to the free ligand, due to the coordination to the metal. It can be seen that the general tendency is a slight displacement to lower energy for the ligands in the complexes in regard to the corresponding free ligand, due to decreased electron density on them when coordinated to the metal. The most marked effect is observed for *[Ru(dmbpy)$_2$((CN)$_2$ppl](PF$_6$)$_2$*, **4**, where the

Table 1
^{1}H NMR chemical shifts (ppm) for all synthesized complexes, in CD_3CN (200 or 400 MHz).

Position	Complexes			
	[Ru(dmbpy)$_2$(OH)$_2$ppl]$^{+2}$ (**1**)	*[Ru(dmbpy)$_2$(COOEt)$_2$ppl]$^{+2}$* (**2**)	*[Ru(dmbpy)$_2$(COOH)$_2$ppl]$^{+2}$* (**3**)	*[Ru(dmbpy)$_2$(CN)$_2$ppl]$^{+2}$* (**4**)
Ha, Ha′	8.64 (s, 2H); J_{ab} = 4.43	8.53 (d, 2H); J_{ab} = 4.92	8.30 (d, 2H); J_{ab} = 8.12	8.41 (dd, 2H); J_{ab} = 5.41, J_{ac} = 1.23
Hb, Hb′	8.13 (m, 2H)	8.01 (dd, 2H); J_{bc} = 8.37, J_{ba} = 4.92	7.93 (dd, 2H); J_{bc} = 8.11, J_{ba} = 5.41	8.05 (dd, 2H); J_{ba} = 5.41, J_{bc} = 8.36
Hc, Hc′	9.59 (d, 2H); J_{ca} = 8.61	9.48 (d, 2H); J_{cb} = 8.37	9.45 (d, 2H); J_{cb} = 8.12	9.58 (dd, 2H); J_{cb} = 8.38, J_{ca} = 1.23
H3	8.81 (s, 2H)	8.58 (s, 2H)	8.36 (s, 2H)	8.57 (s, 2H); J_{35} = 1.23
H3′	8.77 (s, 2H)	8.63 (s, 2H)	8.40 (s, 2H)	8.60 (s, 2H); $J_{3'5'}$ = 1.23
H5	7.30 (d, 2H); J_{56} = 4.92	7.09 (d, 2H); J_{56} = 5.17	7.07 (d, 2H); J_{56} = 5.66	7.15 (dd, 2H); J_{53} = 1.23, J_{56} = 5.91
H5′	7.54 (d, 2H); $J_{5'6'}$ = 5.16	7.36 (d, 2H); $J_{5'6'}$ = 5.41	7.30 (d, 2H); $J_{5'6'}$ = 5.17	7.38 (dd, 2H); $J_{5'6'}$ = 5.56
H6	7.91 (d, 2H); J_{65} = 4.92	7.68 (d, 2H); J_{65} = 5.17	7.44 (d, 2H); J_{65} = 5.66	7.55 (dd, 2H); J_{65} = 5.91
H6′	8.07 (d, 2H); $J_{6'5'}$ = 5.16	7.86 (d, 2H); $J_{6'5'}$ = 5.41	7.62 (d, 2H); $J_{6'5'}$ = 5.17	7.71 (dd, 2H); $J_{6'5'}$ = 5.56
CH_3	2.58 (s, 6H)	2.50 (s, 6H)	2.57 (s, 6H)	2.61 (s, 6H)
CH'_3	2.48 (s, 6H)	2.39 (s, 6H)	2.48 (s, 6H)	2.52 (s, 6H)
CH_2		4.47 (m, 4H)		
CH'_2		1.93 (d, 4H)		

Table 2
UV–Vis spectroscopic data for *[Ru(dmbpy)$_2$R$_2$ppl](PF$_6$)$_2$* complexes in acetonitrile.

Complexes	λ_{max} (nm)	
	IL	TCML
1	259, 284, 338	433, 457
2	265, 282, 354	442
3	260, 283, 337	450
4	259, 284, 337	446
[Ru (dmbpy)$_2$ppl](PF$_6$)$_2$[a] (**5**)	256, 285	450
[Ru (dmbpy)$_2$(COOMe)ppl](PF$_6$)$_2$[a] (**6**)	259, 284	447
[Ru(dmbpy)$_2$Cl$_2$[b] (**7**)	296	377, 560

[a] Ref. [22].
[b] Ref. [27].

tension signal of the CN group at 2223 cm^{-1}, shifts 23 cm^{-1} to lower energy respect to the free ligand, reflecting a probable loss of the triple bond character in CN, due to back bonding effects.

The UV–Vis spectra of all complexes show a similar structure, with bands around 280 and 300 nm, which can be ascribed to spin-allowed ligand-centered (IL, $\pi\rightarrow\pi^*$ and $n\rightarrow\pi^*$) transitions, associated with polypyridine units present in the complexes. The shoulder of lower intensity at 320–380 nm can be assigned to intraligand ($\pi\rightarrow\pi^*$) transitions in the *R$_2$ppl* moiety overlapped with intrametal transitions [24].

Table 2 summarizes the data obtained for the UV–Vis spectra of complexes **1**–**4**. Results from comparable complexes are also shown. All of the complexes display bands in the 400–500 nm range, which are of MLCT (metal-to-ligand charge transfer) character, with λ_{max} at 450–460 nm (extinction coefficient ε in the order of 10^4 M^{-1} cm^{-1}), without any appreciable resolution of transitions involving different ligands. By comparing complexes **1**–**4** with similar reported complexes, it can be observed that, as is typical in Ru(II)–polypyridine complexes [22], the energy of the intraligand bands are not affected by the substituent on the *dmbpy* or *ppl* ligands. The MLCT bands do not change significantly, although there is a certain tendency. A more detailed analysis of the absorption bands and their assignment can be achieved by a theoretical characterization of the complexes, as follows.

Table 3 shows TDDFT results for the simulated absorption spectra. In general all the complexes exhibit two electronic transitions with oscillator strength between 0.08 and 0.20, with the exception of complex **3** where three signals are observed. Electronic excitations are displayed in column 6 and their assignments are proposed in column 7.

A transition density study[21] (Tables S1–S4) was performed using the above data, revealing that the absorption bands of complexes **1**–**4** contain mostly MLCT bands from the metal to the donor ligand (M→L). This contribution corresponds to about 50–80% of the band. Additionally, 20–30% of this band is due to MLCT bands to the corresponding acceptor ligand (M→LA or M→BQ). Finally, a small contribution of ligand to ligand (LL) bands also exists, which only becomes important for complex **3** (R = COOH).

3.4. Electrochemical properties of complexes *1*–*4*

Table 4 shows the electrochemical results for the series of complexes. Data for other Ru(II)–polypyridine complexes are included for comparison purposes.

Table 3
Comparison of TDDFT calculations with UV–Vis spectroscopic data of complexes **1**–**4**, recorded in acetonitrile.

Complexes	λ_{max} (Exp)	λ_{max} (Calc)	Oscillator strength	Electronic transition	Main excitations	Assignment
1	457	451	0.10	1A	41% H2→L1	MBL
					37% H1→L2	ML
					9% H2→L	MBL
					7% H3→L2	MB
		443	0.17	1B	34% H2→L2	ML
					17% H1→L1	MBL
					13% H2→L12	ML
					11% H1→L	MB
					10% H→L3	MB
					5% H1→L4	MQ
2	442	433	0.09	2A	44% H2→L3	ML
					35% H1→L11	MB
					16% H1→L2	ML
		429	0.11	2B	37% H1→L3	ML
					27% H3→L3	ML
					21% H2→L11	MB
					5% H4→L	QL
					4% H2→L2	ML
3	450	433	0.09	3A	44% H2→L3	ML
					35% H1→L4	MBQ
					15% H1→L2	ML
		432	0.06	3B	48% H3→L3	LL
					34% H1→L3	ML
					9% H2→L4	MBQ
		428	0.07	3C	51% H3→L3	LL
					25% H1→L3	ML
					15% H2→L4	MBQ
					4% H2→L2	ML
4	446	436	0.11	4A	32% H5→L	ML
					29% H1→L4	ML
					28% H2→L2	MB
					9% H→L5	MB
		432	0.08	4B	52% H6→L4	ML
					43% H10→L	ML
					2% H→L6	ML

H = HOMO, H1 = HOMO − 1, L = LUMO, L1 = LUMO + 1.
Metal to ligand charge transfer excitations: ML = metal to ligand (L = dmbpy), MB = metal to the bipyridine fragment (B), MQ = metal to quinoxaline fragment (Q), MBL = metal to B and L, MBQ = metal to B and Q fragments; LL = ligand to ligand excitation.

Table 4
Electrochemical properties of $[Ru(dmbpy)_2R_2ppl](PF_6)_2$ complexes, vs. SCE in CH_3CN.

Complexes[a]	$E_{1/2,ox}$ (V)	$E_{1/2,red}$ (V)
1	1.22	−0.95[c], −1.11[c]
2	1.28	−0.89, −1.19, −1.47
3	1.29	−0.87, −1.18
4	1.30	−0.86
$[Ru(dmbpy)_2\ ppl]^{2+}$[b] (**5**)	1.24	−1.23
$[Ru(dmbpy)_2(COOMe)ppl]^{2+}$[b] (**6**)	1.29	−0.96
$[Ru(dmbpy)_3]^{2+}$[b] (**7**)	1.09	−1.47

[a] As PF_6^- salt.
[b] Ref. [22].
[c] $E_{p,red}$, irreversible processes.

Comparison of the $E_{1/2,ox}$ and $E_{1/2,red}$ values of complexes **1**–**4** with the homoleptic $[Ru(dmbpy)_3]^{2+}$compound **7**, demonstrate that R_2ppl acts as acceptor ligand in these complexes. The electron-withdrawing effect of R_2ppl produces a decrease in the electron density on the Ru, making its oxidation more difficult. The reduction process is more sensitive to this effect, decreasing $E_{1/2,red}$ down to approximately 0.5 V with respect to **7**. In complexes **1**, **2** and **3** more than one process of reduction was observed. In complex **1**, both reduction processes are irreversible. In all cases, the first and second reduction process was assigned to the R_2ppl acceptor ligand. In complex **2** the third process was assigned to the *dmbpy* ligand, by comparison with **7**.

The values of $E_{1/2,red}$ for the first reduction of complexes **2**, **3** and **4** show no significant difference. Nevertheless, the effect of R substituents COOEt, COOH, CN is important when compared to complex **5** (R = H). On the other hand, as expected, by comparing the $E_{1/2,red}$ values of **2** and **6**, the effect of electron density reduction produced by two substituent groups on **2** is greater than that of one substituent in **6**; thus **2** is more easily reduced. In complex **1** the reduction process is irreversible, so it is not possible to compare it with other complexes.

When the oxidation processes are considered, the effect of the different R substituents in the *ppl* ligand on the values of $E_{1/2,ox}$ is insignificant, the major difference being 0.08 V. Nevertheless, the comparison of the $E_{1/2,ox}$ values for complexes **2**, **3** and **4** with that for **5** shows that the electron-acceptor effect of the R substituents hinders the metal oxidation respect to R = H. In complex **1** the OH group produces a slight decrease of $E_{1/2,ox}$ due to the electron-donor character of the OH group relative to H. By comparing **2** with **6** there is no significant effect on the $E_{1/2,ox}$ value associated with the number of ester substituents in the *ppl* ligand.

In addition, according to the results discussed above for the corresponding complexes, the electron-acceptor ability of the disubstituted *ppl* ligands increases in the following order:

$$ppl < (COOEt)_2ppl < (COOH)_2ppl < (CN)_2ppl$$

4. Theoretical studies

4.1. Molecular orbital calculations of the free ligands

As mentioned in Scheme 2 of Section 2.3, the *ppl* ligand can be described as the sum of bipyridine and quinoline fragments [27,30]. The molecular orbital calculations performed for the series of ligands under study reveals that the HOMO is composed mainly of atomic orbitals from the nitrogen atom of the bipyridine fragment (**B**), with the exception of the hydroxo ligand, where the HOMO is degenerate and contains contributions from the (**B**) and (**Q**) fragments. Looking at the LUMO's, it can be mentioned that all of them are centered on the quinoxaline fragment (**Q**), as shown in Fig. 4.

It is noteworthy that for ligands R = H and R = OH, the LUMO + 1 molecular orbital is centered on the (**B**) fragment, while for the other ligands of the series, which contain an acceptor group, the electron density is centered on the (**Q**) fragment.

4.2. Electrophilicity index

Since these ligands play the role of anchors when used in solar cells, it is important to analyze their capacity to concentrate electron density. This can be achieved by means of the electrophilicity index [31], $E = \frac{\mu^2}{2\eta}$ where μ is the chemical potential, identified with the HOMO eigenvalue and η is the global hardness [32], which can be calculated as half of the energy difference between the HOMO and SOMO molecular orbitals. Results are displayed in Table 5 and include values for the 4,4′-dicarboxylic acid-2,2′-bipyridine (*dcbpy*), and *dmbpy* ligands. The first of them is introduced as a reference acceptor compound since it is widely employed as anchor group while the latter is known for its donating ability.

Fig. 5 confirms the observed trend that *dcbpy* is a better electron acceptor than *dmbpy*, which is reflected by its higher electrophilicity (7.2 versus 5.4 eV). It can also be observed that *ppl* is located between these values (6.4 eV) and when the OH moiety is introduced in the pyrazine ring, a slight decrease (to 6.3 eV) of its acceptor capacity occurs. On the other hand, COOMe, COOH and CN substituent groups clearly enhance the acceptor capacity of the *ppl* ligand. Indeed the $(CN)_2ppl$ is the most electrophilic of the whole series. The general trend observed for the increase of electrophilicity follows the sequence:

$$(OH)_2ppl < ppl < (COOMe)_2ppl < (COOH)_2ppl < (CN)_2ppl$$

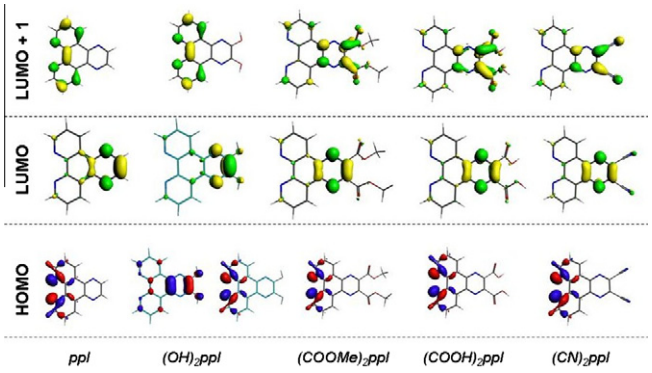

Fig. 4. Isodensity plots for HOMO, LUMO and LUMO + 1 molecular orbitals of R_2ppl free ligands (R = H, OH, COOMe, COOH, CN).

Table 5
Theoretical characterization of the acceptor capacity of the R_2ppl ligands.

R_2ppl	ε_{HOMO} (eV)	ε_{SOMO} (eV)	μ (eV)	η (eV)	E (eV)
OH	−9.91	−2.17	−9.91	7.74	6.34
H	−10.01	−2.21	−10.01	7.80	6.42
COOMe[a]	−10.20	−2.91	−10.20	7.30	7.14
COOH	−10.40	−3.07	−10.40	7.28	7.36
CN	−10.70	−3.71	−10.70	7.00	8.19
Reference ligands					
dmbpy	−9.55	−1.09	−9.55	8.46	5.39
dcbpy	−10.34	−2.90	−10.34	7.44	7.19

[a] Although experimentally COOEt was used, for simplicity the calculations were performed for COOMe.

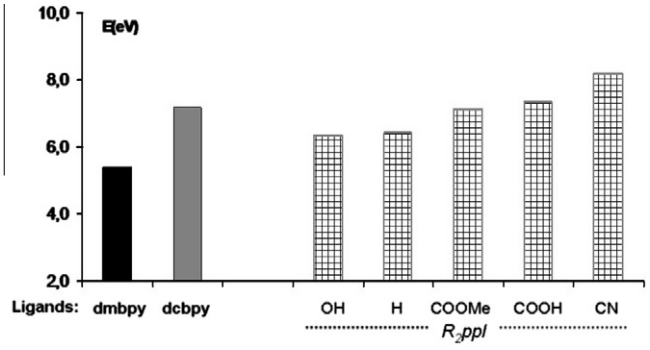

Fig. 5. Electrophilicity Index of *dcbpy*, *dmbpy* and R_2ppl ligands (R = H, OH, COOMe, COOH, CN).

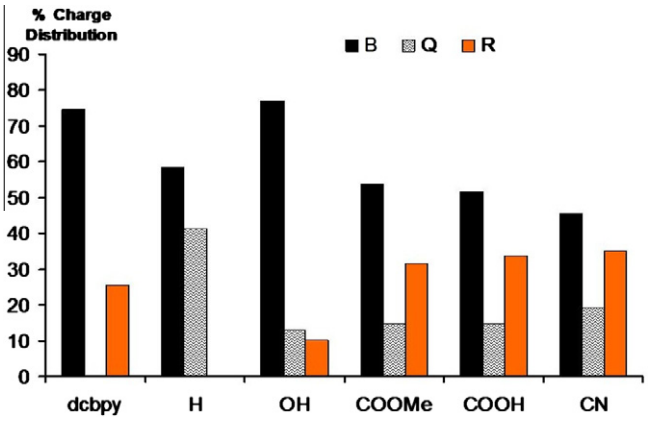

Fig. 6. Charge distribution on the fragment components of the reduced free ligands.

Since the chemical potential remains relatively constant along the series, the increase of the electron-acceptor capacity must be governed by the reduction of the band gap caused by a stabilization of the LUMO/SOMO molecular orbital.

4.3. Reduced charge distribution of ligands

Another interesting aspect to analyze is the effectiveness of the substituent in the *ppl* ligand to concentrate charge and, therefore, to increase its potentiality to inject electron density to the semiconductor conduction band. It should be noted that in this type of molecules, charge analysis indicates that the nitrogens in bipyridine as well as those in pyrazine are negatively charged, and, therefore, compete with the acceptor group(R) in the R_2ppl ligand to attract electronic charge.

It is important to analyse the charge distribution that would be observed if an extra electron is received by the ligand, as occurs *via* MLCT bands, when the ligand forms part of a ruthenium complex. Fig. 6 shows this distribution along the component fragments defined in Scheme 2. For example, on the *dcbpy* ligand, 71% of the electronic charge is located on the bipyridine fragment (**B**) and 29% on the carboxylated moiety (**R**). A different pattern is observed on *ppl* (R = H), which contains the quinoxaline fragment (**Q**) that stores 40% of the total charge. The hydroxyl moiety of the $(OH)_2ppl$ ligand clearly diminishes the acceptor capacity of the quinoxaline fragment. The ability of carbonyl and cyano R groups to attract electronic density is evident since they concentrate 34% and 35% of the total charge. It is interesting to note that a consequence of the increase of the electron density on the quinoxaline (as for example in the dicyano ligand) is that its basicity also increases, opening the possibility of side reactions that could affect the performance of the dye in the cell, as has been pointed out previously [33].

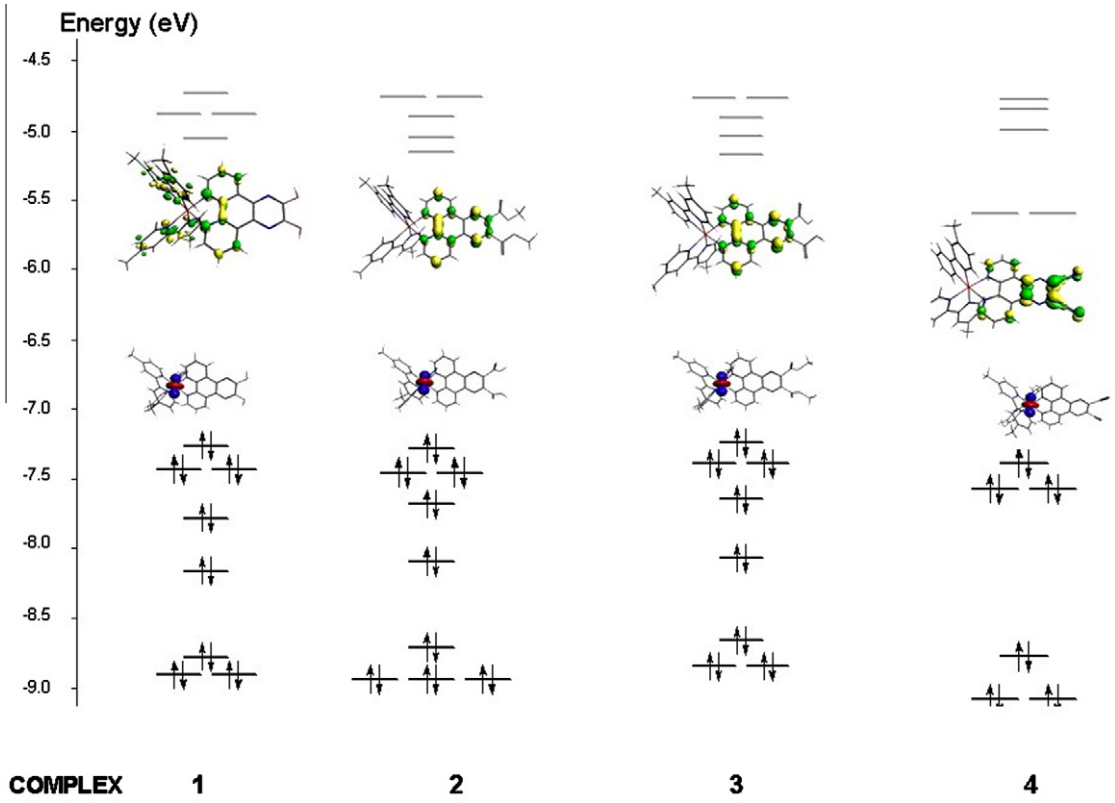

Fig. 7. Molecular orbital Scheme for complexes **1**–**4**.

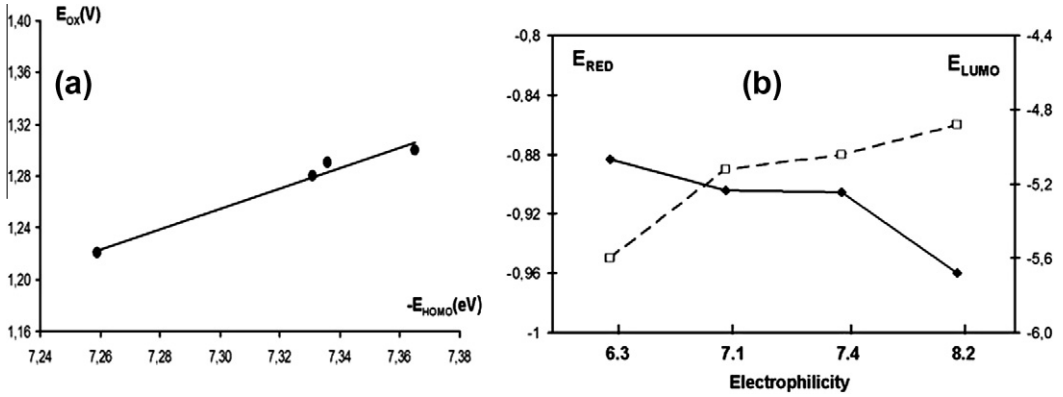

Fig. 8. (a) correlation between the HOMO energy (eV) and the first oxidation potential (V) and (b) influence of the ligand's electrophilicity (eV) on the LUMO energy (•, eV) and on the first reduction potential (°, V).

Table 6
Calculated values of I_T for $[Ru(dmbpy)_2R_2ppl](PF_6)_2$ complexes.

Complexes	E_A	ζ(BQ)	Φ_T(Q)	I_T
1	1.31	0.30	0	0
2	1.12	0.29	0.30	0.10
3	1.89	0.23	0.31	0.14
4	1.10	0.21	0.52	0.12
$[Ru(dcbpy)(bpy)_2]^{2+}$	1.87	0.41	0.83	0.64

4.4. Molecular orbital calculations of the complexes

The HOMO and LUMO molecular orbitals were calculated for the set of ruthenium compounds $[Ru(dmbpy)_2R_2ppl]^{2+}$ (R = OH, COOMe, COOH, CN) under study, Fig. 7.

It can be seen that all the HOMO′s are centered on the metal orbitals with a small contribution of the ligands (3%) for the case of R = H and OH. Fig. 8(a) shows the correlation between the energy of the HOMO level and the first oxidation potential. A linear correlation coefficient of 0.98 is found. Fig. 7 shows that the LUMO of the complexes is mainly the result of the contribution of two molecular fragments, one centered in the bipyridine (**B**) and the other on the quinoxaline fragment (**Q**). Complete data is given in Tables S5–S8, Supplementary material. Electron donor substituents such as OH localize electronic density in the bipyridine ring of *ppl*, while electron-acceptor substituents such as CN and COOH display it on the quinoxaline ring. It should be pointed out that the electronic distribution in the LUMO of the complexes shows some differences in regard to the free ligands, Fig. 4. Specifically, upon coordination, the metallic center seems to stabilize the **B** fragment (located mainly on the LUMO + 1 in the free ligand, Fig. 4), turning it part of the LUMO of the corresponding Ruthenium complexes. The influence of ligand's electrophilicity on the LUMO level and on the first reduction potential is depicted in Fig. 8(b). It can be seen that the increase of electrophilicity correlates with a stabilization of the energy of the LUMO level; accordingly, the reduction potential of the series of ligands follows the trend expected by the electrophilic character of the ligand.

4.5. Theoretical evaluation of the complexes as dye sensitizer

The I_T parameter *i.e.* the amount of energy that can be delivered to TiO_2 from the acceptor anchoring ligand in the *thexi* state (see Section 2) was calculated for complexes **1**–**4**, Table 6. Also introduced in this table are data for a reference model complex, $[Ru(dcbpy)(bpy)_2]^{2+}$, with the aim of checking the response of the I_T parameter with a well known dye, with structural similarities to the compounds of these series.

It can be thought that a c relatively higher I_T value can be related to a better performance of the dye in the cell. According to this, among the complexes studied in this work, complex **3**, bearing the $(COOH)_2ppl$ ligand, would be the most efficient dye, while in complex **1**, it is predicted that no injection would occur. The main difference between complex **3** and complexes **2** and **4** is the absorbed energy (E_A) and also the contribution of the anchor to the *thexi* state, Φ_T(Q), with the highest value (0.52) for complex **4**. The relatively high value of the absorbed energy for complex **3** can be attributed to the presence of 33% of ligand to ligand, LL, electronic transition (Table 3, excitations 3B and 3C), value that in the case of the other three complexes does not exceed 3% (Tables S1–S4). Preliminary IPCE results show that compound **3** has the best response as dye in a solar cell.

5. Concluding remarks

In this article the synthesis and complete characterization of a series of ligands of type R_2ppl (R = OH, COOEt, COOH and OH) and their corresponding $[Ru(dmbpy)_2R_2ppl](PF_6)_2$ complexes is reported. Elementary analyses, IR and ^{1}H NMR spectroscopic results are consistent with the proposed molecular structures.

Experimental and theoretical studies were carried out in order to evaluate the effect of the acceptor R substituent on the properties of the *ppl* ligands and complexes. In particular, as the complexes are intended to be used as dyes in DSSCs, their potential injection capacity on the semiconductor surface was estimated. The results indicate that when R = CN, COOH or COOEt, an increase in the electron-acceptor capacity of the *ppl* ligand is observed, which can be theoretically estimated in terms of the electrophilicity parameter. The general trend shown is:

$$(OH)_2ppl < ppl < (COOMe)_2ppl < (COOH)_2ppl < (CN)_2ppl$$

The same trend was observed experimentally for the oxidation potential, while the inverse tendency was detected for the reduction potential.

An analysis of the charge distribution on the SOMO orbitals of the complexes allowed for an insight on how the extra electron received by the ligand through MLCT absorption is distributed. The carbonyl and cyano substituent group son complexes **3** and **4**attract electronic density and concentrate 34–35% of the total charge received. This is reflected in the I_T parameter, that quantifies the potential injection capacity of the complexes, and which has the highest values for these two complexes. Nevertheless in complex **4**, the increase of the electron density on the quinoxaline opens the possibility of alternative deactivation routes, which could affect the performance of the dye in the cell. In this way, of

the four complexes studied in this work, complex **3** appears to be potentially the most promising dye to be used in a photoelectrochemical solar cell.

Acknowledgement

The support of Fondecyt through Project Grants 1020517 and 1110991 is gratefully acknowledged.

Appendix A. Supplementary data

Supplementary data associated with this article can be found, in the online version, at http://dx.doi.org/10.1016/j.poly.2012.12.003.

References

[1] S. Caramori, V. Cristino, R. Boaretto, R. Argazzi, C.A. Bignozzi, A. Di Carlo, Int. J. Photoenergy 2010 (2010) 1.
[2] M.K. Nazeeruddin, E. Baranoff, M. Grätzel, Sol. Energy 85 (2011) 1172B.
[3] M. Grätzel, Inorg. Chem. 44 (2005) 6841.
[4] M.K. Nazeeruddin, P. Péchy, T. Renouard, et al., J. Am. Chem. Soc. 123 (2001) 1613.
[5] F. Gajardo, A.M. Leiva, B. Loeb, A. Delgadillo, J.R. Stromberg, G.J. Meyer, Inorg. Chim. Acta 361 (2008) 613.
[6] (a) G.J. Meyer, J. Photochem. Photobiol. A 158 (2003) 119;
(b) B.V. Bergeron, G.J. Meyer, J. Phys. Chem. B 107 (2003) 245.
[7] (a) K. Kalyanasundaram, M. Grätzel, Coord. Chem. Rev. 177 (1998) 347;
(b) K. Murakoshi, G. Kano, Y. Wada, S. Yanagida, H. Miyazaki, M. Matsumoto, S. Murasawa, J. Electroanal. Chem. 396 (1995) 27.
[8] O.V. Prezhdo, W.R. Duncan, V.V. Prezhdo, Acc. Chem. Res. 41 (2008) 339.
[9] (a) V. Duprez, M. Biancardo, F.C. Krebs, Sol. Energy Mater. Sol. Cells 91 (2007) 230;
(b) P. Piotrowiak, E. Galoppini, Q. Wei, G.J. Meyer, P. Wiewio, J. Am. Chem. Soc. 125 (2003) 5278;
(c) O. Taratula, J. Rochford, P. Piotrowiak, E. Galoppini, R.A. Carlisle, G.J. Meyer, J. Phys. Chem. B 110 (2006) 15734.
[10] (a) I. Gillaizeau-Gauthier, F. Odobel, M. Alebbi, R. Argazzi, E. Costa, C.A. Bignozzi, P. Qu, G.J. Meyer, Inorg. Chem. 40 (2001) 6073;
(b) S. Ardo, G.J. Meyer, Chem. Soc. Rev. 38 (2009) 115.
[11] (a) Y. Qin, Q. Peng, Int. J. Photoenergy 2012 (2012) 21;
(b) M.K. Nazeeruddin, S.M. Zakeeruddin, J.-J. Lagref, P. Liska, P. Comte, C. Barolo, G. Viscardi, K. Schenk, M. Gräetzel, Coord. Chem. Rev. 248 (2004) 1317.
[12] (a) T. Kinoshita, J.-I. Fujisawa, J. Nakazaki, S. Uchida, T. Kubo, H. Segawa, J. Phys. Chem. Lett. 3 (2012) 394;
(b) S. Altobello, R. Argazzi, S. Caramori, C. Contado, S. Da Fré, P. Rubino, C. Choné, G. Larramona, C. Contado, C.A. Bignozzi, J. Am. Chem. Soc. 12 (7) (2005) 15342.
[13] (a) E. Galoppini, Coord. Chem. Rev. 248 (2004) 1283;
(b) M.K. Nazeeruddin, R. Humphry-Baker, P. Liska, M. Grätzel, J. Phys. Chem. B 107 (2003) 8981.
[14] R. López, B. Loeb, T. Boussie, T.J. Meyer, Tetrahedron Lett. 37 (1996) 5437.
[15] (a) B.P. Sullivan, D.J. Salmon, T.J. Meyer, Inorg. Chem. 17 (1978) 3334;
(b) P.A. Lay, A.M. Sargeson, H. Taube, Inorg. Synth. 24 (1986) 24.
[16] G. Velde, F.M. Bickelhaupt, S.J.A. Van Gisbergen, C. Fonseca Guerra, E.J. Baerends, J.G. Snijders, T.J. Ziegler, Comput. Chem. 22 (2002) 931.
[17] J.P. Perdew, Y. Wang, Phys. Rev. B 45 (1992) 13244.
[18] F.L. Hirshfeld, Theor. Chim. Acta 44 (1977) 129.
[19] O. Gritsenko, P. Schipper, E. Baerends, Chem. Phys. Lett. 302 (1999) 199.
[20] A. Klamt, G. Schüürmann, J. Chem. Soc., Perkin Trans. 2 (1993) 799.
[21] F. Gajardo, M. Barrera, R. Vargas, I. Crivelli, B. Loeb, Inorg. Chem. 50 (2011) 5910.
[22] A. Delgadillo, P. Romo, A.M. Leiva, B. Loeb, Helv. Chim. Acta 86 (2003) 2110.
[23] M.A. Ivanov, M.V. Puzyk, K.P. Balashev, Russ. J. Gen. Chem. 76 (2006) 843.
[24] B. Gholamkhass, K. Koike, N. Negishi, H. Hori, K. Takeuchi, Inorg. Chem. 40 (2001) 756.
[25] A. Ambroise, B.G. Maiya, Inorg. Chem. 39 (2000) 4264.
[26] M.D. Stephenson, T.J. Prior, M.J. Hardie, Cryst. Growth Des. 8 (2008) 643.
[27] R. Díaz, A. Francois, M. Barrera, B. Loeb, Polyhedron 39 (2012) 59.
[28] R. Díaz, A. Francois, A.M. Leiva, B. Loeb, E. Norambuena, M. Yañez, Helv. Chim. Acta 89 (2006) 1220.
[29] D.P. Strommen, P.K. Mallick, G.D. Danzer, R.S. Lumpkin, J.R. Kincaid, J. Phys. Chem. 94 (1990) 1357.
[30] E. Norambuena, C. Olea-Azar, A. Delgadillo, M. Barrera, B. Loeb, Chem. Phys. 359 (2009) 92.
[31] R. Parr, L. Szentpaly, S. Liu, J. Am. Chem. Soc. 121 (1999) 1922.
[32] R. Parr, W. Yang, Density-Functional Theory of Atoms and Molecules, Oxford University Press, New York, 1989.
[33] M. Arias, Complejos polipiridínicos de Ru (II) con ligandos altamente conjugados con ancla fosfonato y compuestos ciclometalados de Ru (II) con ancla carboxilato, Thesis to obtain the Dr. Degree in Chemistry, P. Catholic University of Chile, 2007.